Investigation of Stall Phenomena using Zonal RANS-LES Simulations

K. Geurts,[*] M. Meinke[†]

Institute of Aerodynamics

RWTH Aachen University

Wüllnerstr. 5a, D-52062 Aachen, Germany

Abstract

A zonal RANS-LES method is presented and applied to the unsteady flow around an airfoil at high angle of attack. The attached boundary layer is simulated by RANS whereas the laminar separation bubble, the laminar-to-turbulent transition, and the trailing-edge separation are computed using LES. The general RANS domain is connected to the LES domain by overlapping regions. The RANS-to-LES transition for the turbulent boundary layer couples a turbulent inflow generation method with controlled forcing to ensure a fast and smooth transition. The transition from LES to RANS applies a reconstruction technique for the turbulent viscosity combined with a forcing layer to attain the correct boundary layer velocity profile in the RANS domain. This fully coupled zonal method is applied to predict the characteristics of an airfoil at high angle of attack, including the unsteady phenomena occurring near stall. The zonal method reduces the computational costs by a factor of 4 and its results show good agreement with the pure LES findings and experimental data.

1   Introduction

Laminar separation bubbles (LSB) and the onset of trailing-edge separation (TES) on an airfoil at high angle of attack strongly influence the flow around an airfoil and the airfoil characteristics such as the maximum lift. For mixed stall-types, where the trailing-edge separation moves upstream and interacts with the LSB before the bubble bursts, unsteady phenomena can be observed [2, 3]. Precise prediction of laminar-to-turbulent transition, the position and size of the LSB, and the position of the turbulent separation point is essential in determining airfoil characteristics.

The standard methods in industry for determining maximum lift are based on Reynolds-averaged Navier-Stokes (RANS) methods and detached-eddy simulations (DES). In most cases, these RANS and DES computations are unable to correctly predict the location and size of the

---

[*]Research Associate, Institute of Aerodynamics, RWTH Aachen University, k.geurts@aia.rwth-aachen.de

[†]Senior Scientist, Institute of Aerodynamics, RWTH Aachen University

separated flow regions since both depend on the RANS model for the turbulent separation from smooth surfaces [10, 8]. These methods are capable of predicting geometry induced separations at surface discontinuities and sharp corners and edges, but have difficulties simulating creeping flow separation due to smooth pressure gradients. Alternatives for both computation methods are direct numerical and large-eddy simulations (DNS and LES). However, the required computer resources limit the industrial implementation of these methods for high Reynolds number flows. The proposed zonal RANS-LES method divides the computation domain in separate RANS and LES regions that can account for the varying complexity of the flow such that the required computer power is significantly decreased. The solutions of RANS and LES are coupled via transition regions [11, 6]. These transitions from the RANS to the LES domain and visa versa are particularly challenging since synthetic turbulent fluctuations have to be generated at the LES inflow boundary, the eddy viscosity needs to be reconstructed at the RANS inflow boundary, and the transition of the pressure and friction coefficients has to be smooth. These issues will be briefly addressed in the following. First, the numerical method, the synthetic turbulence generation method, and the turbulent viscosity reconstruction are described. Then, the results for the HGR-01 research airfoil at a high angle of attack are presented. The findings of the fully coupled zonal RANS-LES computation are compared with a pure LES simulation for the same configuration. Unlike the RANS simulations described in [17] the LES and the zonal RANS-LES approach yield highly accurate results, reproducing the unsteady phenomena at an angle of attack near stall.

2 Numerical method and boundary conditions

2.1 Flow Solver

The Navier-Stokes equations for three-dimensional unsteady compressible flow are solved by a block-structured finite-volume flow solver. The influence of the subgrid scales are modeled using the MILES (monotone integrated LES) approach [1] . A modified AUSM (advective upstream splitting method) scheme [7] with second-order accuracy is used for the Euler terms. The temporal integration is done by a second-order explicit 5-stage Runge-Kutta method. A detailed description of the fundamental flow solver is given by Meinke *et al.* [9] . The Spalart-Allmaras [15] turbulence model is used for the RANS solution. The RANS and LES domains use periodic boundary conditions in the spanwise direction. Non-reflective boundary conditions are applied at the far field boundaries, and at the airfoil surface, the no-slip boundary condition is imposed at an adiabatic wall.

2.2 Zonal RANS-LES Method

The zonal RANS-LES computation exists of separate overlapping RANS and LES domains. The LES domains are chosen to be as small as possible to reduce the number of grid points required without decreasing the local accuracy. Due to the small LES domains, the LES inflow boundaries are subject to large pressure gradients. At the overlapping in- and outflow boundaries, a sponge/forcing layer is applied to realise a smooth transition between RANS and LES and visa versa. To also ensure a smooth transition from the three-dimensional unsteady LES solution to the two-dimensional RANS solution, another sponge/forcing layer is applied to

damp high frequency pressure and velocity fluctuations at the overlapping region from the LES domain to the RANS domain. Further details of such a sponge layer can be found in Zhang *et al.* [18] .

3   Validation of Zonal Method

3.1   LES-to-RANS Boundary

When going from an LES to a RANS domain, a relevant value for the eddy viscosity is required at the inflow boundary of the RANS domain. This value is reconstructed at the inflow plane using the $k-\omega$ turbulence model [6] . The quantity ω is computed from the normal components of the Reynolds stress tensor using Bradshaw's hypothesis. The turbulent kinetic energy k is determined from the transport equation.

The turbulent boundary flow over a flat plate is used to validate this turbulent viscosity reconstruction method. Fig. 1(a) shows the velocity profiles from a pure LES, a pure RANS, a zonal RANS-LES computation, and the theoretical solution. The numerical distributions are similar. They deviate slightly from the theoretical solution in the outer log region. This behavior is common for low Reynolds number flows. Furthermore, the skin-friction coefficient c_f of the numerical simulations are compared to that of the theoretical friction resistance distribution in Fig. 1(b). The pure LES possesses a somewhat wavy distribution originating from the rescaling method. Downstream of the zonal RANS inflow boundary, the friction coefficient shows a slight overshoot, converging to the other numerical and theoretical solutions further downstream. The flat plate flow computation validates the capability of the turbulent viscosity reconstruction method. Using an overlapping region between the LES and RANS grid, a smooth transition from the spatially to the temporally averaged solution can be obtained.
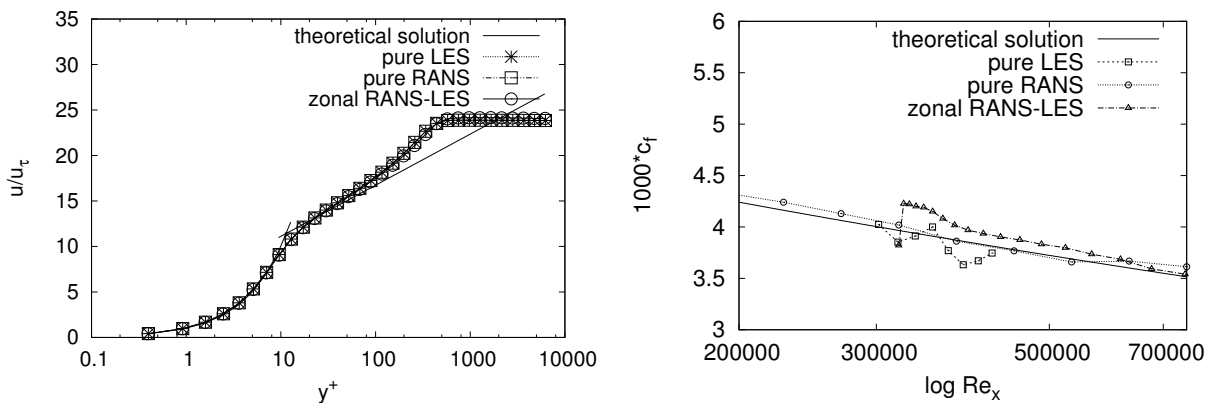
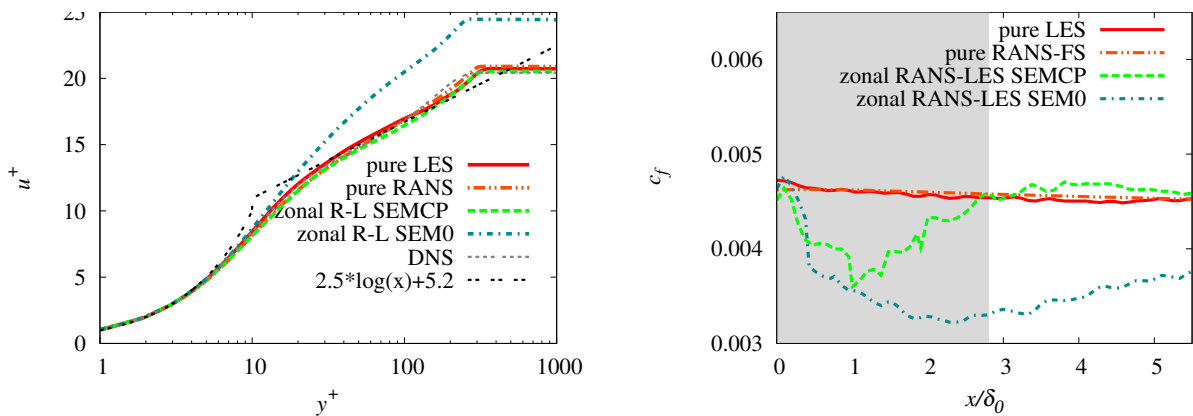(a) Velocity profile downstream of the LES-to-RANS transition

(b) Skin-friction coefficient

Figure 1: Pure LES, pure RANS, and the zonal RANS-LES distributions of a turbulent boundary layer over a flat plate compared to theoretical data.

3.2 RANS-to-LES Boundary

At the inflow of the LES domains, the turbulent boundary layer is reproduced using synthetic turbulence. The synthetic turbulence generation method of Jarrin *et al.* [5] is based on a super-position of coherent structures. Applications of the synthetic-eddy method (SEM) suffer from a long transition length for realistic turbulence generation. Therefore, the idea of Keating [11] to apply controlled forcing [16] to shorten this turbulence development region downstream of the LES inflow boundary is applied. The local control planes of Spille and Kaltenbach [16] intro-duce a volume forcing term to the Navier-Stokes equations to control the turbulence production in the boundary layer and reduce the required overlapping length of the different computational domains. The zonal RANS-LES method was successfully validated by Roidl *et al.* [13, 12] . Furthermore, the turbulent flow over a flat plate is used to investigate the influence of the control planes on the overlapping length between the RANS and LES calculation domains. Fig. 2(a) shows the time and spanwise averaged velocity profiles at $x/\delta_0 = 3$, i.e., three inflow boundary-layer thicknesses downstream of the inflow boundary of the pure LES and embedded LES of the zonal RANS-LES configuration. The velocity profiles of the zonal RANS-LES with control planes (SEMCP) exhibit a satisfying agreement compared to the pure LES. The zonal RANS-LES results without control planes (SEM0) show a large deviation due to the fact that the flow field is still in a transitional state as the flow requires a longer adjustment region. Overall, the velocity distributions of the pure LES, pure RANS, and zonal RANS-LES SEMCP match the DNS data of Schlatter *et al.* [14].

The streamwise development of the skin-friction coefficient distribution is presented in Fig. 2(b). The c_f-distributions of the zonal RANS-LES SEMCP converge to the pure LES solution at about three boundary layer thicknesses downstream of the inflow boundary. Without the vol-ume forcing the c_f-distributions of the zonal RANS-LES simulation drop significantly and do not recover within the streamwise limits of the computational domain due to the lack of infor-mation about the shape and the spectral content of the synthetic eddies that is provided by the SEM.

(a) Velocity profile downstream of the RANS-to-LES transition

(b) Skin-friction coefficient

Figure 2: Pure LES, pure RANS, and zonal RANS-to-LES distributions of a turbulent boundary layer over a flat plate compared to theoretical data.

4   HGR-01 Profile

The near stall flow phenomena of the HGR-01 research airfoil were studied at several angles of attack [17] . In this study, the configuration at an angle of attack of 12° with a laminar separation bubble and trailing-edge separation is simulated at a Reynolds number of $Re_c = 0.65 \cdot 10^6$ based on the chord length c. The high angle of attack flow over the HGR-01 profile is a very demanding test case for hybrid and zonal numerical computations. The flow field consists of a high pressure gradient in front of the leading edge, a small laminar separation bubble with laminar-to-turbulent transition at the leading edge, a critical positive pressure gradient on the upper surface and a trailing-edge separation of about 10%.

The complexity of this test case for a zonal RANS-LES approach not only lies in the simulation of the different flow phenomena but also in positioning the embedded LES domains and the transition from the RANS-to-LES domains and vice versa. These transition regions are located at positions in the flow where different conditions exist, such as laminar and turbulent flow and both positive and negative pressure gradients. One LES domain encompasses the leading edge to capture the LSB and the laminar-to-turbulent transition. A second LES region is located at the trailing edge to accurately predict the highly unsteady behavior of the TES. The rest of the computational domain is resolved by a RANS grid. An overview of the grid lay-out around the HGR-01 airfoil can be found in Fig. 3.
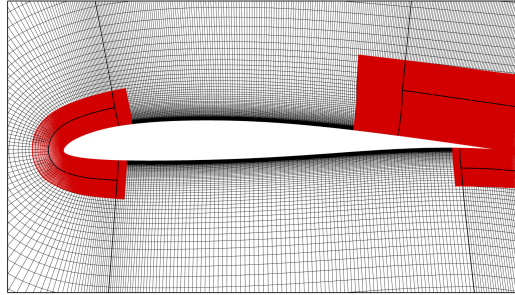

Figure 3: Zonal grid (red/fine = LES, black/coarse = RANS)

The grid resolution for the pure LES computation and the LES domain of the zonal RANS-LES simulation is chosen according to Zhang *et al.* [18]. The resolution of the pure LES grid in the streamwise, wall normal, and spanwise direction of $\Delta x^+ \approx 100$, $\Delta y^+_{min} \approx 1$ and $\Delta z^+ \approx 20$, respectively, results in a mesh with $51.4 \cdot 10^6$ grid points. The spanwise extension of the grid is $0.02\,c$. Using the same grid resolution and spanwise extension for the LES domains in the zonal RANS-LES grid, the total number of grid points was reduced by a factor of 4 to $13.2 \cdot 10^6$ grid points.

5   Results

The flow dynamics simulated in the LES domains around the leading edge and the trailing edge are visualized in Fig. 4. The LSB and the laminar-to-turbulent transition are visualized by λ_2 structures in Fig. 4(a). The vortex shedding of the LSB is clearly visible as well as the three-dimensionality of the flow downstream of the transition. Fig. 4(b) visualizes the flow at the trailing-edge separation and the large vortex structures in the wake.

For a proper averaging of the large scale structures due to the unsteady behavior of the TES,
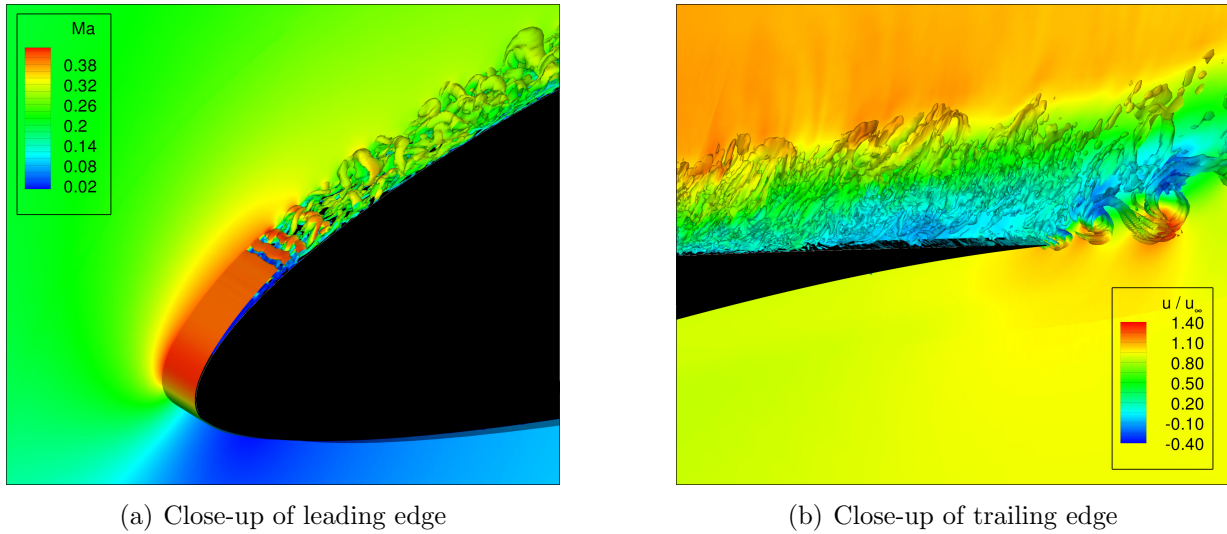

(a) Close-up of leading edge

(b) Close-up of trailing edge

Figure 4: λ_2 structures of the zonal RANS-LES computation showing the LSB and laminar-to-turbulent transition at the leading edge and the turbulent separation at the trailing edge, with mapped-on Mach number and streamwise velocity, respectively.

the zonal computation as well as the pure LES computation require data samples of about 2 c/U_∞ for the velocity profiles and 5 c/U_∞ for a smooth pressure distribution.

Fig. 5 shows the averaged pressure coefficient c_p. The grey shaded areas represent the embedded LES domains around the leading and trailing edge. A smooth transition from the LES to the RANS, and the RANS to the LES zone can be observed. The suction peak with the laminar separation bubble evidenced by the experimental data is nicely reproduced by the LES region within the zonal RANS-LES simulation and the pure LES computation.

The skin-friction coefficient c_f is plotted in Fig. 6 and again shows a comparison between the pure LES computation and the zonal RANS-LES computation. The zonal computation accurately reproduces the wall-shear stress distribution of the leading and trailing edge and the lower surface of the HGR-01 profile. In the center section of the upper surface, where the RANS domain encounters a positive pressure gradient, the skin-friction coefficient slightly deviates from the pure LES results. This will be discussed more profoundly when the RANS velocity profiles are discussed.

The velocity profiles in Fig. 7 are located at several streamwise positions on the upper surface of the HGR-01 airfoil in the embedded LES domains. The profiles from left to right represent the LSB at $0.012\,c$, the velocity profile just upstream of the RANS inflow boundary at $0.12\,c$, and three profiles in the trailing edge LES region, i.e. at $0.68\,c$, $0.85\,c$, and $0.95\,c$. At the leading edge, the zonal computation accurately reproduces the pure LES velocity profiles. The LSB is determined somewhat smaller by the zonal method. Note that the velocity profile at $0.12\,c$ is the profile that is transferred to the RANS inlet boundary. It coincides with the pure LES velocity profile, showing the accurate simulation of the leading edge flow, the LSB, and the laminar-to-turbulent transition.

At the trailing-edge separation region, the results of the averaged zonal RANS-LES and the pure LES are compared with particle-image velocimetry (PIV) data [17] to validate the numerical results. The PIV results depend on the spanwise position and show a small three-dimensional effect in the TES. The maximum span s of the experimentally investigated airfoil is $3.25\,s/c$ and
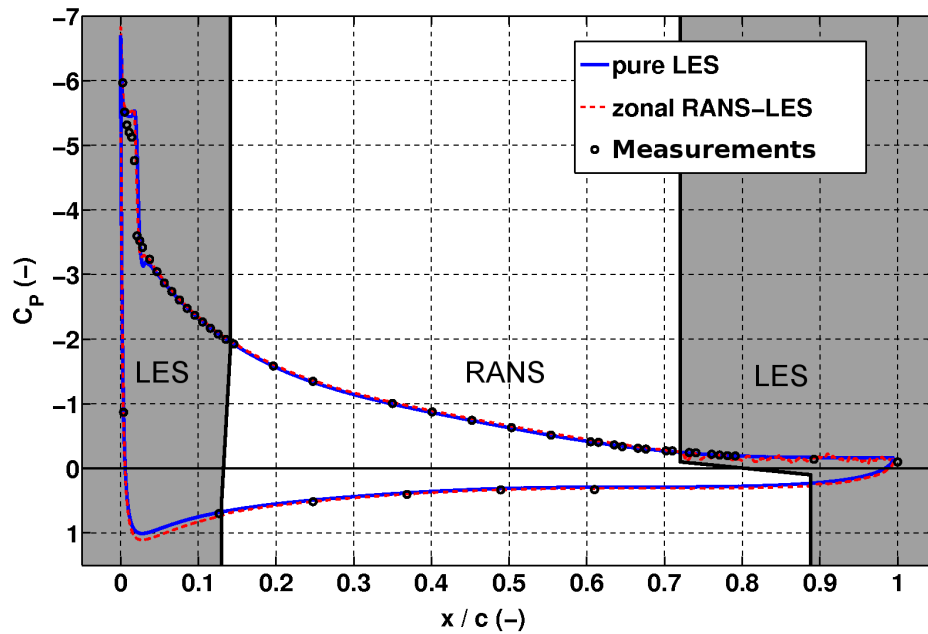
Figure 5: Pressure coefficient c_p at the upper and lower surface of the HGR-01 airfoil for the zonal RANS-LES, pure LES computations, and experiments [17] .
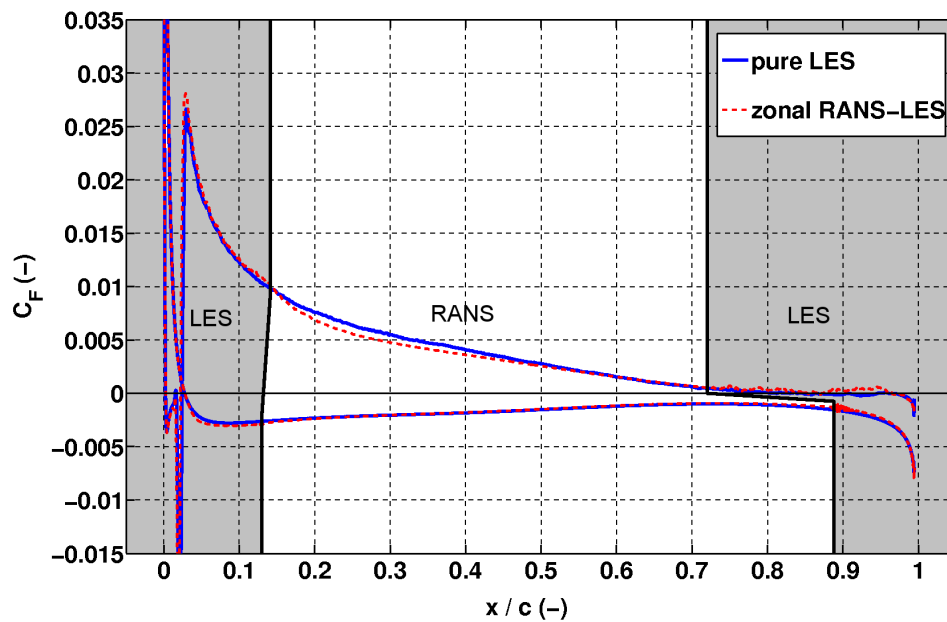

Figure 6: Skin-friction coefficient c_f at the upper and lower surface of the HGR-01 airfoil for the zonal RANS-LES and pure LES computations.

the visualized PIV results represent the velocity profiles at 1.6, 1.9, and 2.6 s/c, respectively. The pure LES computation shows very good agreement with the PIV measurements. Looking closely at the velocity profiles at the trailing edge, it should be noted that the zonal velocity profiles deviate somewhat from the reference LES computation. They are fuller near the surface and the boundary-layer thickness is smaller. This difference does not have a significant influence on the pressure and friction coefficient. From the velocity profiles it can be seen that the deviation already exists at $0.68\,c$.
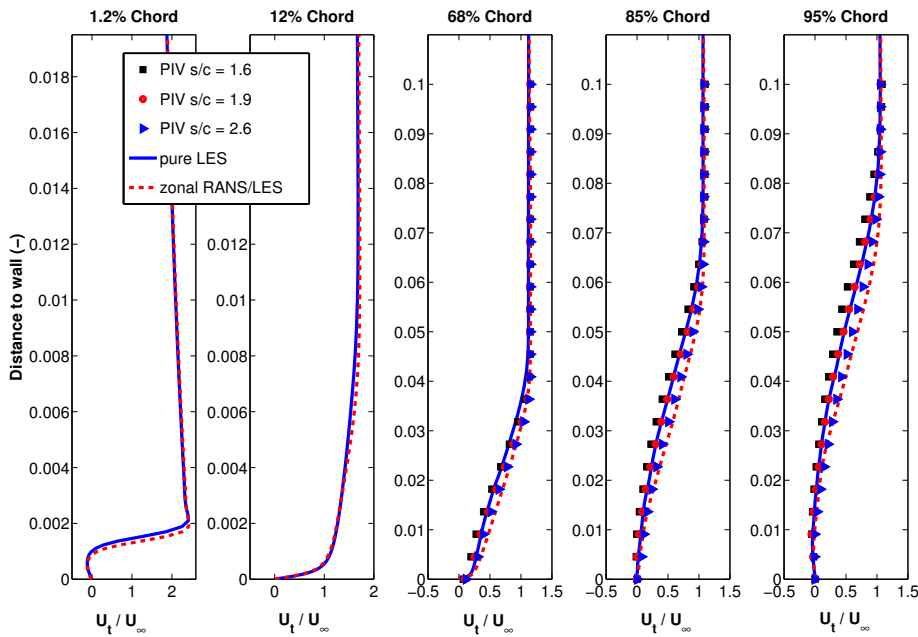

Figure 7: Velocity profiles at several streamwise positions for zonal RANS-LES, pure LES computations, and experiments.

Starting at the overlapping region at the leading edge, where large pressure gradients over the domain edges exist, the pressure and Mach number are plotted on a grid line near the stagnation streamline in Figs. 8(a) and 8(b). The transition is sufficiently smooth to guarantee a correct simulation of the incoming flow at the leading edge.

A close-up of the pressure coefficient at the LSB is presented in Fig. 9(a). The accurate simulation of the LSB at the leading edge is essential for the flow dynamics of the entire airfoil. The difficulty comes from the position of the LES inflow boundary upstream of the leading edge, i.e., in the freestream, with a large negative pressure gradient from the incoming flow. The close-up clearly visualizes the ability of the zonal method to capture the position and length of the LSB. The small deviation with respect to the experiments is due to the lack of freestream turbulence in the pure LES and the zonal computation.

From the pressure distribution in Fig 9(a) and the skin-friction coefficient in Fig. 9(b) it can be seen that the LSB is slightly shorter than for the pure LES data, however, still somewhat longer than the experimental data. The skin-friction coefficient also shows a slightly smaller negative friction peak at the end of the LSB, indicating the smaller height of the bubble as seen from the velocity profile.

Looking more closely to the velocity profiles and Reynolds stress tensor profiles somewhat
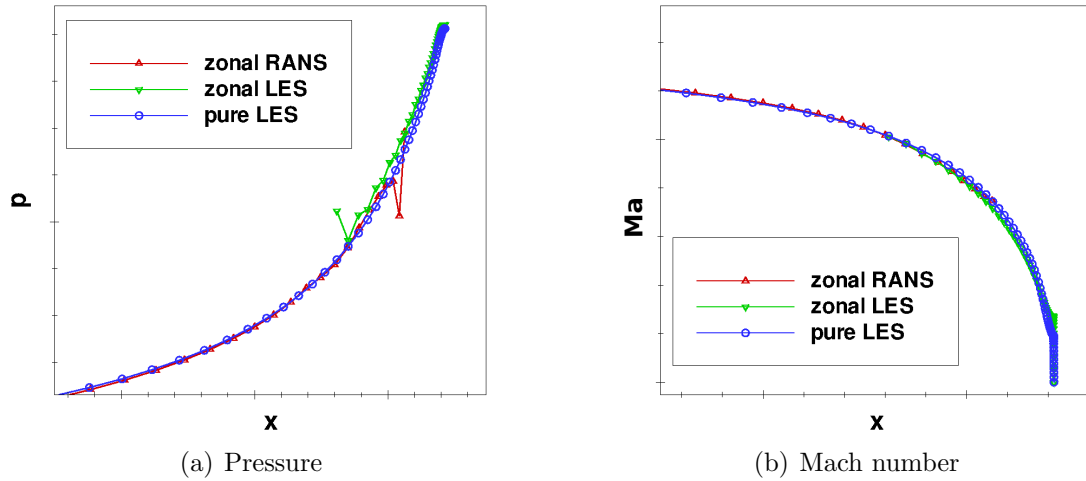
(a) Pressure

(b) Mach number

Figure 8: Streamwise development of the pressure and Mach number along a grid line near the stagnation streamline, showing the transition from RANS to LES.
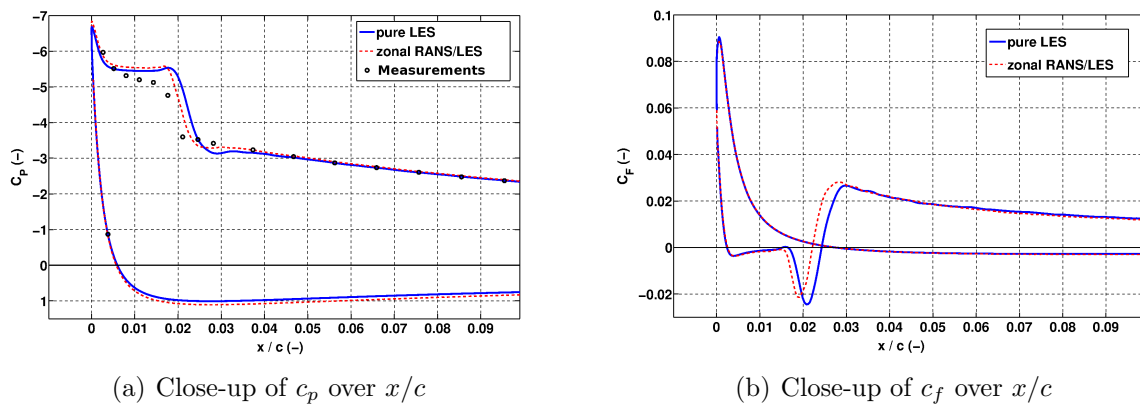

(a) Close-up of c_p over x/c

(b) Close-up of c_f over x/c

Figure 9: Pressure coefficient c_p and skin-friction coefficient c_f close-up of the leading edge of the HGR-01 airfoil for the zonal RANS-LES and pure LES computations.

downstream of the LSB at $0.045\,c$ in Fig. 10 and $0.12\,c$ in Fig. 11 it can be seen how this bubble height influences the RMS values of the velocities. Their profiles, which are scaled by the boundary layer thickness δ_0, show a smaller turbulent intensity than the pure LES. The difference in intensity for u_{RMS} and v_{RMS} decreases further downstream. The time averaged velocity and Reynolds shear stress $< u'v' >$ profiles are not influenced by the height difference. The velocity profiles and Reynolds shear stress in the RANS domain on the upper surface are
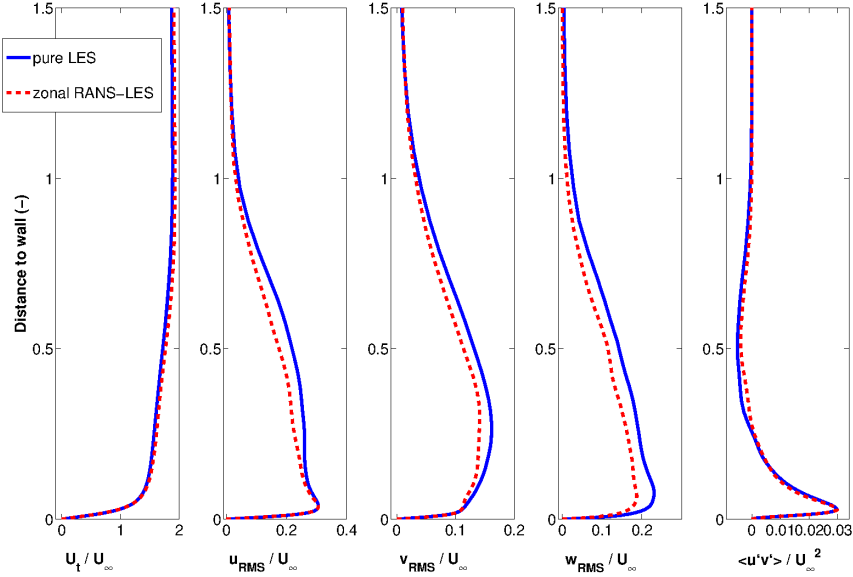

Figure 10: Velocity and Reynolds stress tensor component profiles at $c/L = 0.045$.

shown in Fig. 12. The results at a streamwise position of $0.30\,c$ show only a slight deviation from the pure LES data. Note that the Reynolds shear stress profile for the zonal computation belongs to an equilibrium boundary layer as opposed to the non-equilibrium state of the pure LES boundary layer. The equilibrium state of the RANS introduces a higher turbulent intensity, in contrast to the higher turbulent energy for the pure LES at $0.12\,c$. This results in an increasing deviation between the pure LES and the zonal RANS results. The velocity profile becomes fuller further downstream at $0.60\,c$, changing the flow characteristics at the suction side of the HGR-01 profile. This is crucial for the inflow boundary conditions of the trailing edge LES region. This effect on the RANS velocity profile was already discussed by Celic and Hirschel [4] .

Fig. 13 shows the influence of the deviating RANS velocity profile on the LES results at the trailing edge. The pure LES velocity profile and the PIV data show the separation onset at about $0.85\,c$. However, the zonal LES shows a positive velocity gradient which decreases the intensity of the flow to separate. This results in a smaller separation region at the trailing edge for the zonal RANS-LES computation. However, as shown before, this deviation has only a limited effect on the pressure and friction resistance distribution.

The significance of this test case is defined by the correct simulation of the LSB together with the laminar-to-turbulent transition plus the trailing-edge separation, since these phenomena influence the flow field around the airfoil and thus the airfoil characteristics such as the lift and drag coefficients. The smaller trailing-edge separation increases the lift coefficient slightly with respect to the pure LES reference computation as shown in Table 1.
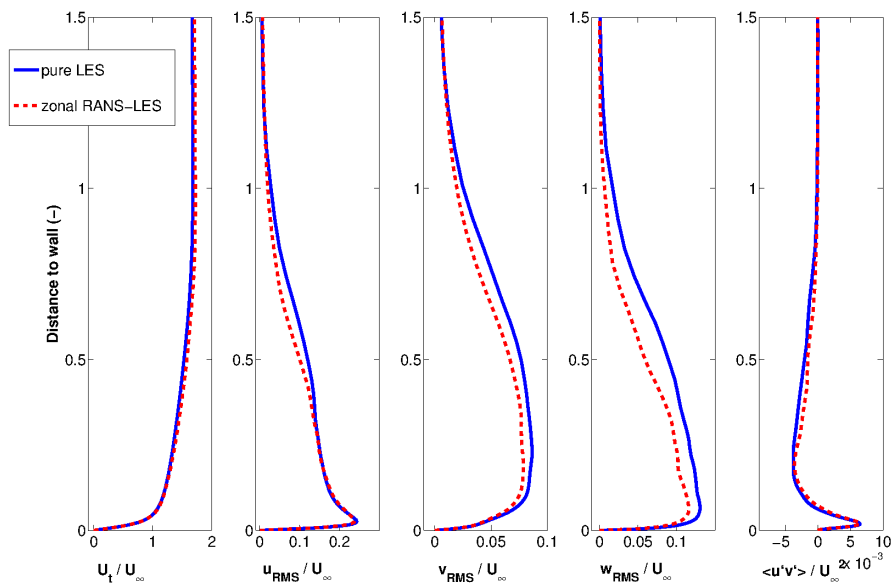
Figure 11: Velocity and Reynolds stress tensor component profiles at $c/L = 0.12$.
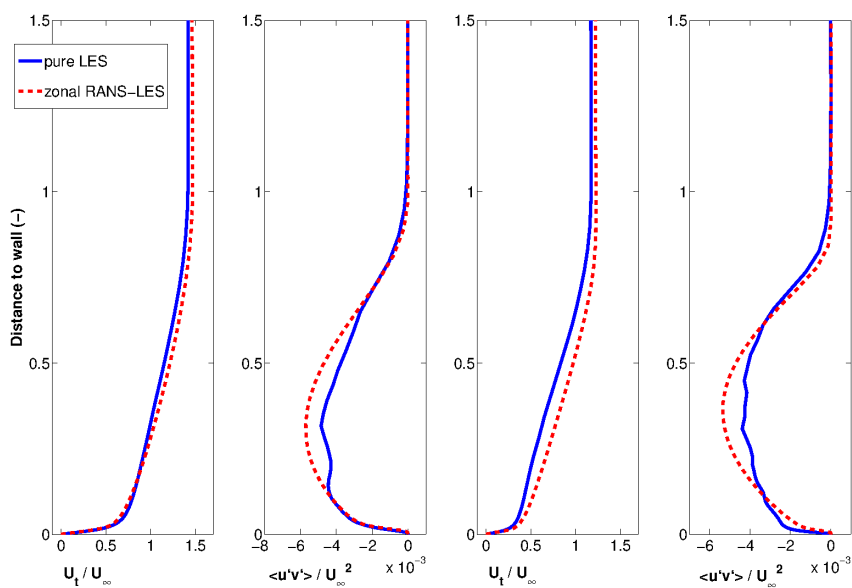

Figure 12: Velocity and Reynolds shear stress profiles at $c/L = 0.30$ (left) and $c/L = 0.60$ (right).
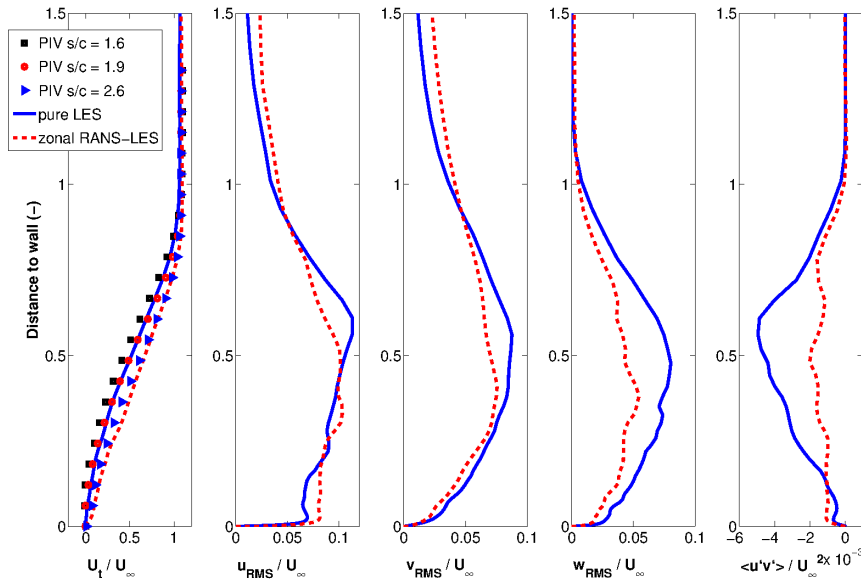
Figure 13: Velocity and Reynolds stress tensor component profiles $c/L = 0.85$.

	LES	ZONAL	Experiments	RANS
Lift C_l	1.366	1.426	1.370	1.530
Drag C_d	0.0403	0.0414	0.032	0.028

Table 1: Lift and drag comparison

The comparison of the characteristic values of the pure LES computation, the experiments, and the RANS data [17] shows that the zonal RANS-LES method delivers more accurate results than the RANS. The drag coefficient resulting from the experiments is determined from pressure probe measurements on the surface. Thus, only the pressure resistance is measured, explaining the difference with the LES and zonal RANS-LES results. The lower drag coefficient for the RANS can be explained by the almost non-existing trailing-edge separation. The RANS overestimates the lift and underestimates the drag due to the fact that the RANS model predicts the turbulent separation point too close to the trailing edge. The accuracy of the zonal computation compared to the LES reference data is determined limited by the RANS limitations at the suction side of the profile.

6   Summary

The zonal RANS-LES method is presented and applied to simulate the flow around an HGR-01 airfoil at high angle of attack. The results are compared with experimental data and pure LES solutions. Averaged pressure and skin-friction coefficients as well as the lift coefficient show good agreement with the LES results. Lift and drag coefficients correspond well with the reference LES computation. The experiments result in the same lift coefficient, but show a slightly smaller trailing-edge separation, and therefore a lower drag coefficient. This test case is especially challenging for turbulence modeling due to the existence of a laminar separation bubble

and a separated flow region at the trailing edge. These unsteady flow phenomena observed in the experiments and the LES simulation are correctly reproduced by the zonal RANS-LES method. The zonal RANS-LES method reduces the computational cost by a factor 4, while approximately maintaining the high accuracy of the pure LES. The RANS limitations for the turbulent boundary layer at the suction side cause the slight deviation of the zonal RANS-LES compared to the pure LES solutions.

References

[1] J. P. Boris, F. F. Grinstein, E. S. Oran, and R. L. Kolbe. New Insights into Large Eddy Simulation. *Fluid Dynam. Res.*, 10:199–228, 1992.

[2] M. B. Bragg, D. C. Heinrich, F. A. Balow, and K. B. M. Q. Zaman. Flow Oscillation over an Airfoil near Stall. *AIAA Journal*, 34(1):199–201, 1996.

[3] A. P. Broeren and M. B. Braghg. Flowfield Measurements over an Airfoil during Natural Low-Frequency Oscillations near Stall. *AIAA Journal*, 37(1):130–132, 1998.

[4] A. Celić and E. H. Hirschel. Comparison of eddy-viscosity turbulence models in flows with adverse pressure gradient. *AIAA J.*, 44(10):2153–2169, 2006.

[5] N. Jarrin, N. Benhamadouche, S. Laurence, and D. Prosser. A synthetic-eddy-method for generating inflow conditions for large-eddy simulations. *Journal of Heat and Fluid Flow*, 27:585–593, 2006.

[6] D. König, M. Meinke, and W. Schröder. Embedded LES/RANS boundary in zonal simulations. *Journal of Turbulence*, 11(7):1–25, 2010.

[7] M. S. Liou and C. J. Steffen-Jr. A New Flux Splitting Scheme. *J. Comp. Phys.*, 107:23–39, 1993.

[8] D. C. Lyons, L. J. Peltier, F. J. Zajaczkowski, and E. G. Paterson. Assessment of DES models for separated flow from a hump in a turbulent boundary layer. *Journal of Fluids Engineering*, 131(11):111203, 2009.

[9] M. Meinke, W. Schröder, E. Krause, and T. Rister. A comparison of second- and sixth-order methods for large-eddy simulations. *Comput. Fluids*, 31:695–718, 2002.

[10] C. Mockett. *A Comprehensive study of detached-eddy simulation*. PhD thesis, Technische Universität Berlin, 2009.

[11] G. D. Prisco, U. Piomelli, and A. Keating. Improved turbulence generation techniques for hybrid RANS/LES calculations. *Journal of Turbulence*, 9:1–20, 2008.

[12] B. Roidl, M. Meinke, and W. Schröder. Zonal RANS-LES computation of transonic airfoil flow. AIAA Paper 2011-3974, 2011. 29th AIAA Applied Aerodynamics Conference, 27-30 June, Honolulu, Hawaii.

[13] B. Roidl, M. Meinke, and W. Schröder. A zonal RANS/LES method for compressible flows. *submittet to Comp. Fluids*, -:–, 2011.

[14] P. Schlatter, R. Örlü, R. Li, G. Brethouwer, J. H. M. Fransson, A. V. Johansson, P. H. Al-fredsson, and D. Henningson. Turbulent boundary layers up to Re_θ=2500 studied through simulation and experiment. *Phys. Fluids*, 21:051702, 2009.

[15] P. R. Spalart and S. R. Allmaras. A One-Equation Turbulence Model for Aerodynamic Flows. AIAA-Paper 92-0439, 1992. 30th Aerospace Sciences Meeting & Exhibit, Jan 6-9, Reno.

[16] A. Spille-Kohoff and H.-J. Kaltenbach. Generation of turbulent inflow data with a pre-scribed shear-stress profile. August 2001. Third AFSOR Conference on DNS and LES.

[17] R. Wokoeck, N. Krimmelbein, J. Ortmans, V. Ciobaca, R. Radespiel, and A. Krumbein. RANS Simulations and Experiments on the Stall Behaviour of an Airfoil with Laminar Separation Bubbles. AIAA Paper 2006-0244, 2006. 44th AIAA Aerospace Sciences Meeting and Exhibit.

[18] Q. Zhang, W. Schröder, and M. Meinke. A zonal RANS/LES method to determine the flow over a high-lift configuration. *Comput. Fluids*, 39:1241–1253, 2010.